Two-Dimensional Room-Temperature Giant Antiferrodistortive $SrTiO_3$ at a Grain Boundary

Bo Han,[1] Ruixue Zhu,[1] Xiaomei Li,[2] Mei Wu,[1] Ryo Ishikawa,[3,4] Bin Feng,[3] Xuedong Bai,[2] Yuichi Ikuhara,[3,5,6] and Peng Gao[1,7,8,*]

[1]*Electron Microscopy Laboratory and International Center for Quantum Materials, School of Physics, Peking University, Beijing 100871, China*

[2]*Beijing National Laboratory for Condensed Matter Physics, Institute of Physics, Chinese Academy of Sciences, Beijing 100190, China*

[3]*Institute of Engineering Innovation, School of Engineering, The University of Tokyo, Tokyo 113-8656, Japan*

[4]*Japan Science and Technology Agency, PRESTO, Kawaguchi, Saitama 332-0012, Japan*

[5]*Nanostructures Research Laboratory, Japan Fine Ceramic Center, Nagoya 456-8587, Japan*

[6]*WPI Advanced Institute for Materials Research, Tohoku University, Sendai 980-8577, Japan*

[7]*Collaborative Innovation Center of Quantum Matter, Beijing 100871, China*

[8]*Interdisciplinary Institute of Light-Element Quantum Materials and Research Center for Light-Element Advanced Materials, Peking University, Beijing 100871, China*

(Received 29 June 2020; accepted 23 April 2021; published 4 June 2021)

The broken symmetry at structural defects such as grain boundaries (GBs) discontinues chemical bonds, leading to the emergence of new properties that are absent in the bulk owing to the couplings between the lattice and other parameters. Here, we create a two-dimensional antiferrodistortive (AFD) strontium titanate ($SrTiO_3$) phase at a $\Sigma 13(510)/[001]$ $SrTiO_3$ tilt GB at room temperature. We find that such an anomalous room-temperature AFD phase with the thickness of approximate six unit cells is stabilized by the charge doping from oxygen vacancies. The localized AFD originated from the strong lattice-charge couplings at a $SrTiO_3$ GB is expected to play important roles in the electrical and optical activity of GBs and can explain past experiments such as the transport properties of electroceramic $SrTiO_3$. Our study also provides new strategies to create low-dimensional anomalous elements for future nanoelectronics via grain boundary engineering.

DOI: 10.1103/PhysRevLett.126.225702

Strontium titanate ($SrTiO_3$) is a prototype perovskite oxide. Besides the excellent dielectric properties, numerous exotic phenomena such as superconductivity [1], two-dimensional (2D) electron gases [2], and blue light emission [3,4] were also discovered in it. Properties of $SrTiO_3$ usually originate from the interplays between two complex competitive driving forces: antiferrodistortive (AFD) and ferroelectric (FE) ordering [5]. As cooling from room temperature to the low critical temperature of 105 K, $SrTiO_3$ undergoes the second order phase transition from cubic symmetry ($Pm\bar{3}m$) toward tetragonal phase ($I4/mcm$), i.e., the AFD phase. Besides low temperature, the AFD order can also be created by chemical doping [6] and at a largely strained interface [7]. Unlike ideal $SrTiO_3$ with an indirect band gap, the AFD phase possesses a direct band structure [8–10], which is also proposed to be the origin of blue light emission [11] and giant photoconductivity [12] in $SrTiO_3$. While the FE order was found to be stabilized by isotope substitution [13], strain [14], and/or reduced size [15] in thin films, and optical pulse [16,17]. Its emergence significantly changes the dielectric and transport properties of $SrTiO_3$ [18]. AFD and FE orders can also coexist in the artificial superlattice [19] and give rise to improper ferroelectricity.

Creation and manipulation of AFD and FE orders are highly desirable to achieve novel optical and electrical properties in otherwise ideal quantum paraelectric $SrTiO_3$. The structural defects such as point defects, dislocations, and grain boundaries (GBs) with broken translation symmetry, have been demonstrated to effectively tune the FE order. For example, the Sr vacancy [20], O vacancy [21], and Ti antisite [22] can generate nanopolarized regions, leading to the emergence of macroscopic FE order in thin films with proper boundary conditions [15]. The dislocations of $SrTiO_3$ also generate local FE order due to the flexoelectric effect [23]. The underlying mechanism can be understood by the discontinued chemical bonds at the defects that disturb the delicate couplings between lattice and charge and thus trigger the phase transition to generate FE order. However, despite extensive studies on defect tuning FE order in $SrTiO_3$, whether the AFD order can be similarly manipulated by structural defects such as dislocations or GBs, remains still largely unknown.

In this work, we reveal the atomic arrangements including oxygen at a $\Sigma13(510)/[001]$ $SrTiO_3$ tilt GB by using atomic-resolution scanning transmission electron microscopy (STEM) imaging combined with energy dispersive x-ray spectroscopy (EDS). We find that, in the vicinity of GB, the $SrTiO_3$ becomes AFD phase with the octahedron rotation angles up to 6° within six unit cells even at room temperature. Atomic-scale electron energy-loss spectroscopy (EELS) indicates that the AFD phase mainly arises from the local presence of oxygen vacancy (V_o), which causes electron doping to the Ti ions and thus expands and rotates the TiO_6 octahedrons. These findings provide explanations for the past optical measurements and transport properties of electroceramic $SrTiO_3$. The ability to obtain anomalous nanosized phases deviating from equilibrium phase diagrams via GB engineering also provides opportunities to design new devices for nanoelectronics.

A high-angle annular dark-field STEM (HAADF STEM) image in Fig. 1(a) shows the atomic structure of a $\Sigma13\,(510)/[001]$ tilt $SrTiO_3$ GB in the present study with each structural unit in the length of five unit cells. Although there is inevitably slight structural variability in the GB core [24], the framework of the GB structure unit remains the same, of which the representative averaged GB core structure is shown in Supplemental Material, Fig. S1 [25]. The atomically resolved elemental maps of STEM-EDS shown in Fig. 1(b) and Supplemental Material, Fig. S2 [25] reveal the atomic arrangements of Sr and Ti atoms near the GB core. The HAADF STEM image and EDS maps are used to distinguish the cation atom species at the GB core. In order to precisely extract the atom position information including oxygen near the GB, the integrated differential phase contrast (IDPC) image is recorded in Fig. 1(c). The IDPC imaging has the capability to visualize light elements with atomic resolution and excellent signal-to-noise ratio at low electron dose [27], allowing us to extract the oxygen positions in a perovskite structure [28], even inside a GB core [29]. Combing with all these imaging and spectroscopies, the atomic structure of the single $SrTiO_3$ $\Sigma13$ unit can be obtained and shown in Fig. 1(d). Intriguingly, the $\Sigma13$ GB core undergoes a localized structural reconstruction, i.e., at some locations [for example, highlighted by the circle in Fig. 1(d)], the pristine perovskite structure of TiO_6 octahedron with corner sharing configuration transforms into rocksaltlike structure with edge sharing configuration. Such localized reconstructions were also found in $SrTiO_3$ dislocations and GBs with other mistilt angles [30] to accommodate the local strain and Sr deficiency. It should be noted that from the STEM imaging and spectroscopies shown above, we cannot fully preclude the possibility for low-level chemical intermixing at each atomic column due to the complex channeling effect and limited detection sensitivity in STEM [31], especially in the GB core region. Nevertheless, no apparent chemical intermixing was observed, indicating chemical intermixing might be slight enough to be negligible [30]. Therefore, the atomic structure shown in Fig. 1(d) can be reasonably recognized as the representative configuration for this GB.

The room-temperature AFD $SrTiO_3$ is identified based on IDPC imaging. Figure 2(a) illustrates the atomic positions of TiO_6 reconstructed by 2D Gaussian fitting (see Material and Methods for details), where Sr atoms and the GB core with more complicated structure are not displayed for clarity. The raw IDPC image is shown in Supplemental Material, Fig. S3 [25]. The TiO_6 octahedron rotations in the vicinity of the GB are pronounced. Every TiO_6 octahedron rotates in the opposite direction with respect to their neighbors. The in-plane octahedral rotation shown in Fig. 2(a) is indicative of an AFD phase. Note that although the structural information along the electron beam direction is unavailable from this projected image, since the basic structure of the AFD phase remains the bulklike

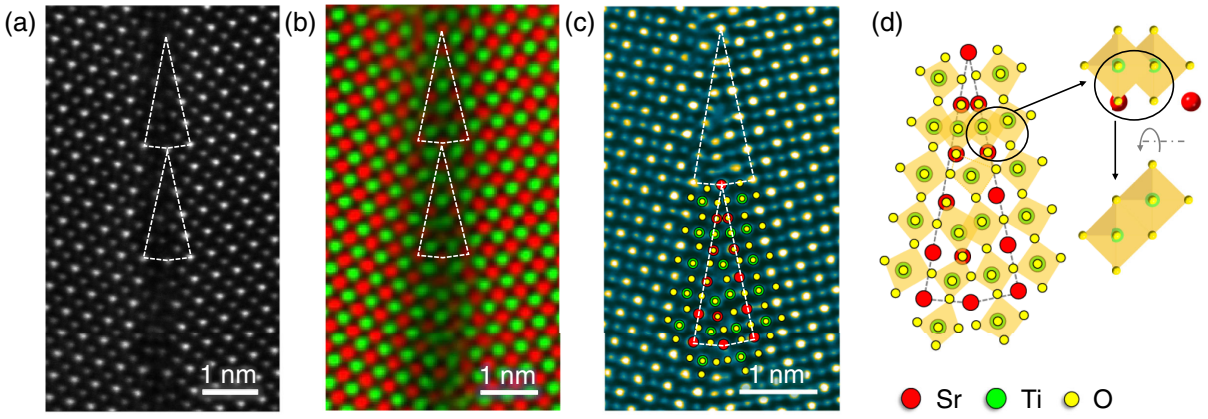

FIG. 1. Atomic structure of a $\Sigma13(510)/[001]SrTiO_3$ GB. (a) A HAADF image of the $SrTiO_3$ $\Sigma13(510)/[001]$ tilt GB. The polygon highlights the structure unit of GB. (b) An EDS map of Sr (red) and Ti (green) showing cationic distribution of the GB. (c) An IDPC image of GB overlapped with an atomistic structure model. (d) An atomistic schematic of the GB. Edge sharing TiO_6 octahedrons with rocksaltlike TiO structure is observed in the GB core.

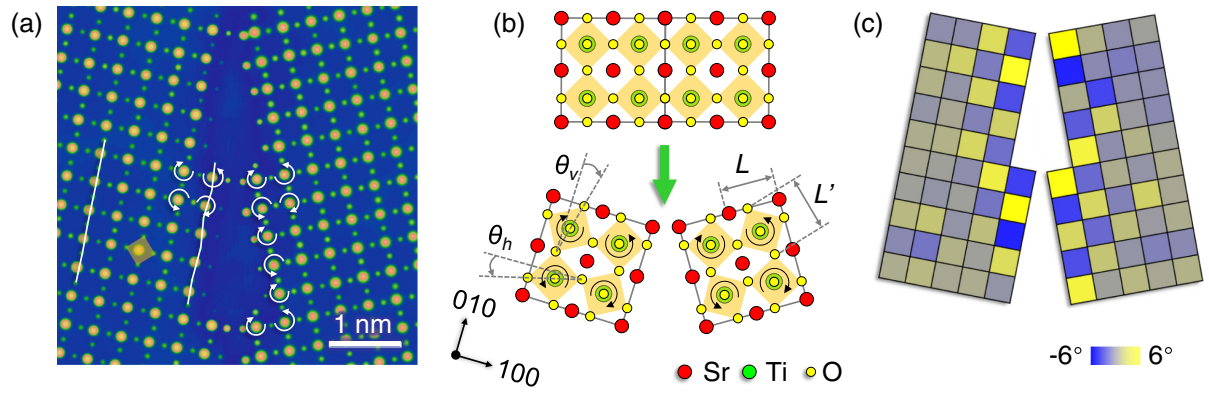

FIG. 2. The room-temperature AFD phase in the vicinity of the $SrTiO_3$ GB. (a) Reconstructed atom positions of Ti and O atoms on the basis of the IDPC image. The Sr atoms and core structure are hidden for clarity. The white lines highlight the O-Ti-O atomic chains. The curved arrows highlight the TiO_6 rotation direction. (b) The schematic diagrams of AFD phase in the vicinity of the GB. The adjacent Ti-O octahedrons tilt to opposite directions, viewing along the [001] zone axis. Size difference between SrO squares (L) and TiO squares (L') lead to the TiO_6 octahedron rotation. The rotation angles of TiO_6 octahedron are illustrated as "vertical" component θ_v (along the [010]) and "horizontal" component θ_h (along the [100]). (c) The θ_v map of TiO_6 octahedrons in the vicinity of $\Sigma 13(510)/[001]$ GB.

structure of $SrTiO_3$, the structure along the projection direction should remain as the regular perovskite structure. Figure 2(b) depicts octahedrons rotation and the definitions of rotation angles θ_h (along the [100]) and θ_v (along the [010]). Size difference between SrO squares (L) and TiO squares (L') contributes to the oxygen octahedron rotations [32]. The unit-cell scale octahedron rotation angle can be calculated using the positions of adjacent O columns [33]. As shown in Fig. 2(c) and Supplemental Material, Figs. S4 and S5 [25], the maximum of the rotation angle is ~6.7° occurring at the edge of the GB core and gradually becomes weaker away from it. The maximum value is consistent with theoretical calculations [34] but larger than the previous experimental values [35]. It is also noteworthy that the AFD phase is generally stabilized only under 105 K [36], whereas our experiments were conducted at room temperature.

To explore the underlying physical origins with respect to the formation of room-temperature AFD, we implemented EELS analysis across the GB. For a Ti^{4+} in $SrTiO_3$, the Ti$-L$ edge typically incorporates four separate peaks, whereas the Ti$-L$ edge of a standard Ti^{3+} spectrum (e.g., Ti in $LaTiO_3$) contains only two broad peaks. Inside the GB core in Figs. 3(a) and 3(b), the Ti$-L$ edge becomes broader accompanied by a less pronounced peak separation, indicating the presence of a decrease in the crystal field splitting feature and an increase in Ti^{3+} fraction [37]. The decrease of $t_{2g}-e_g$ splitting of Ti$-L$ edge [Fig. 3(c)] implies a change in Ti-O coordination [38]. The O$-K$ edge in the vicinity of GBs becomes flat due to the disruption of symmetry and loss of local order [Figs. 3(d) and 3(e)], which could be caused by the presence of the V_o [39]. According to the previous study [40], the distortions of Ti-O-Ti linear chains in $SrTiO_3$ would enhance the intensity of the peak β, leading to a reduced α/β intensity ratio as marked in Fig. 3(e). In other words, α/β ratio also reflects the degree of TiO_6 octahedron distortion. As demonstrated in Fig. 3(f), the largest distortions of TiO_6 octahedrons exist inside the GB core due to the broken translational symmetry and large structural variation. In the AFD phase, the relatively small α/β ratio is attributed to the TiO_6 rotation.

The variation of the local crystal field can be estimated by fitting the Ti$-L$ edge, of which the fine structures are very sensitive to the local atomic environments. We use Ti$-L$ edges in $SrTiO_3$ (Ti^{4+}) and $LaTiO_3$ (Ti^{3+}) as references (detailed in Fig. S6 [25]). The experimentally obtained Ti$-L$ edges in EELS are fitted as linear combinations of them [41]. As shown in Fig. 3(g), far away from the GB core (~1.2 nm or ~3 unit cells), the crystal field remains the bulk $SrTiO_3$ (Ti^{4+}), while inside the GB core it is very similar to that of $LaTiO_3$ (Ti^{3+}). This can be understood by the presence of localized rocksalt phase with the lower Ti valence state since the ratio $Ti:O = 1:1$ in the rocksalt structure is much lower than that of 1:3 in the perovskite. In fact, an increase of $Ti/O \sim 40\%$ occurs inside the GB core from Figs. 3(h) and 3(i), which cannot be simply attributed to the oxygen deficiency in perovskite and thus further underpin that a decrease in crystal field splitting at the GB core is mainly due to the structural transformation from the perovskite to the rocksalt. In the AFD region approaching the GB core, the crystal field gradually changes from $SrTiO_3$ (Ti^{4+}) to $LaTiO_3$ (Ti^{3+}) features. Besides, the intensity ratio between Ti$-L_2$ and Ti$-L_3$ (L_2/L_3) in the AFD region also gradually decreases from the bulk $SrTiO_3$ to the GB core. According to the previous study [42], such a decrease in the intensity ratio corresponds to the reduction of Ti valence (see Fig. S7 for details).

Since the structure of AFD still remains to be perovskite, the change of the crystal field is likely due to the presence of oxygen vacancies (V_o). The electrons offered by the V_o

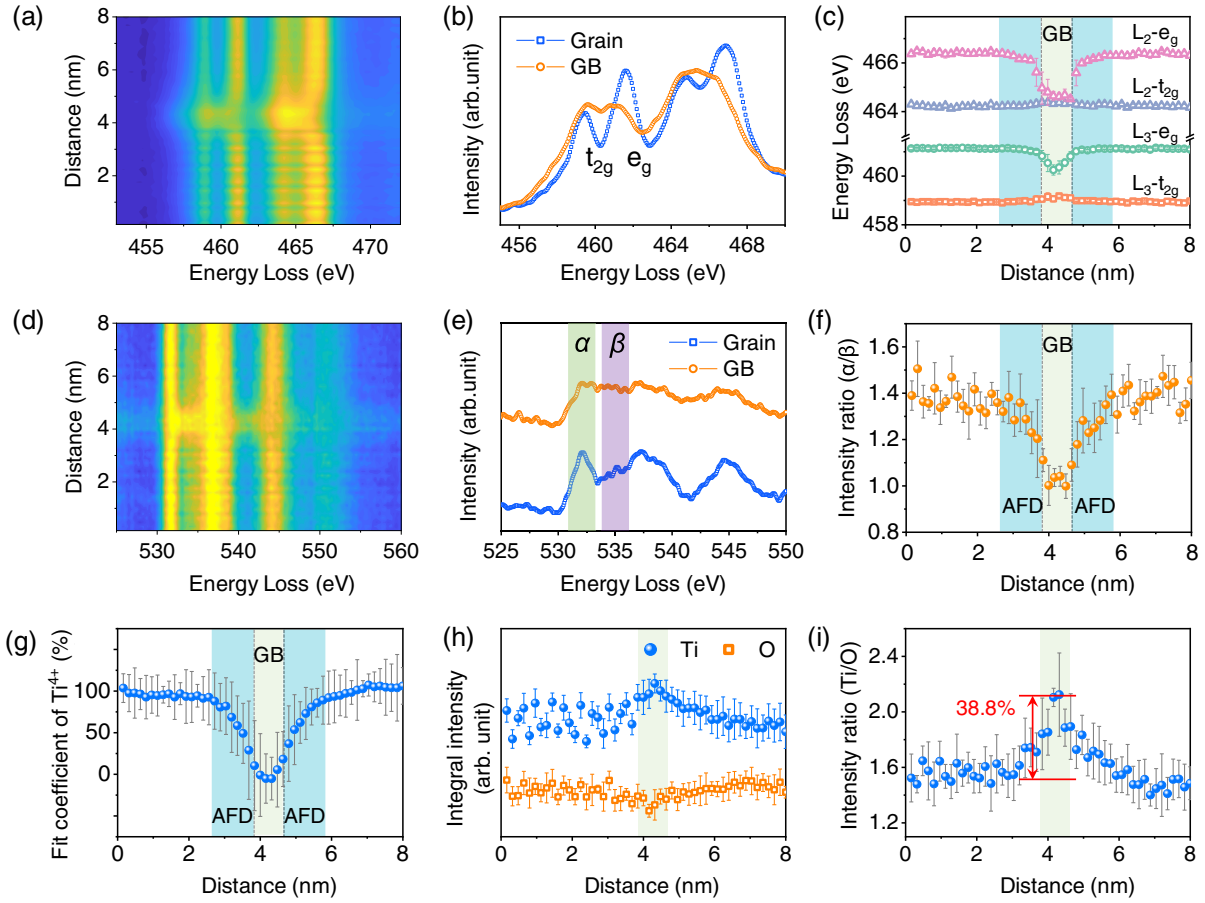

FIG. 3. Electronic structures of the $SrTiO_3$ near the GB. (a) EELS of Ti$-L$ edge within a range of 8 nm across a GB. (b) A comparison in EELS between bulk matrix and GB indicated by blue and orange doted lines, respectively. (c) The energy-loss values of peaks in Ti$-L$ edge across the GB. (d) The corresponding O-K edge across the GB. (e) The comparison between bulk matrix and GB. Green and purple shades label the windows used to calculate (f) the α/β intensity ratio. Reseda green and indigo shades indicate the GB core and AFD phase regions, respectively. (g) The fitting coefficient of Ti^{4+} across the GB. (h) The intensity of Ti$-L$ and O$-K$ and (i) their relative ratios after background subtracted. The error bars present the standard deviations among ten groups of line-scan measurements from a single EELS spectrum image containing ten rows datasets across the GB (10×50 pixels mapping).

occupy Ti $3d$ states, leading to the valence reduction of Ti^{4+} accompanied with the alter of crystal field. Meanwhile, the decrease in the valence of Ti yields the expansions of Ti ionic radii, thus increasing the size of TiO_6 octahedron (L') and facilitating the octahedral rotation. Indeed, V_o can promote the formation of AFD, which was theoretically predicted [11,43]. Therefore, controllably introducing high density of V_o via reducing gases or high vacuum during bicrystal fabrication may further facilitate the AFD at room temperature.

The presence of AFD provides new insights into understanding the complex interplay of $SrTiO_3$ GBs. The broken translation symmetry at the GB is validated to modify the internal driving forces, overcome the temperature barrier, and stabilize the AFD phase in $SrTiO_3$ within a region of about six unit cells in thickness even at the room temperature, demonstrating the capability to create anomalous nanosized phases with simple defect engineering in the complex oxides. Considering the AFD phase also undergoes the strain field induced by the GB (see Fig. S8 for GPA analyses) [25], the TiO_6 rotation in AFD phase may introduce a rotostriction effect, i.e., the coupling between the TiO_6 rotation and strain, which may further generate a polarization similar to that at AFD domain walls [44] and twin boundaries [45].

The presence of AFD associated with oxygen vacancies is expected to play important roles in determining the electrical and optical properties of the GBs of $SrTiO_3$. In fact, the oxygen deficiency at the GBs of $SrTiO_3$ has been proposed in many studies [46,47]. However, the origin of such deficiency has still been under debate, i.e., whether it comes from the localized second phase or simply nonstoichiometric perovskite. Our observations give a deterministic picture, i.e., oxygen deficiency around the GBs of $SrTiO_3$ mainly comes from the V_o of perovskite while inside the GB core it is dominated by the presence of localized rocksalt phase. The positive charge such as oxygen vacancies around the GB accounts for the

formation of space charge zone with hole depletion, leading to formation of back-to-back Schottky barrier at the GBs in the electroceramic $SrTiO_3$ [48,49]. Therefore, the presence of the AFD phase unambiguously underpins the oxygen vacancy associated hole depletion model and can explain many past experimental results such as high-ionic impedance and nonlinear electrical activity [50,51]. Moreover, AFD phase was reported to yield extra localized electronic states in the band gap [11] and enhance its luminescence efficiency [4]. Since the AFD phase has a direct band gap unlike paraelectric $SrTiO_3$ with an indirect band gap [10], the 2D GB likely offers a higher photoconductivity [12] as the zero-momentum transfer benefits for phototransition. We therefore expect that a 2D AFD phase along the GB plane could be fabricated into "photoconductive channels," offering an alluring prospect in nanophotonic devices.

In summary, we reveal the atomic structure including the oxygen configuration of a $SrTiO_3$ $\Sigma 13(510)/[001]$ tilt GB, and find a 2D AFD $SrTiO_3$ phase in the vicinity of GB at room temperature. Such an AFD order likely originates from the localized V_o induced electron doping. The presence of the hole depletion AFD at the GB also explains the past transport and optical properties in the electroceramic $SrTiO_3$. Furthermore, the AFD phase that is not expected at room temperature but can be created via GB engineering of ordinary $SrTiO_3$, provides new opportunities to design novel nanoelectronic and nanophotonic devices, especially considering that the AFD phase exhibits a 2D nature with width only approximate six unit cells.

This work was supported by the National Key R&D Program of China (2016YFA0300804), the National Natural Science Foundation of China (11974023, 52021006), the Key R&D Program of Guangdong Province (2018B030327001, 2018B010109009), the National Equipment Program of China (ZDYZ2015-1), and the "2011 Program" from the Peking-Tsinghua-IOP Collaborative Innovation Center of Quantum Matter. Part of this study was supported by a Grant-in-Aid for Specially Promoted Research (Grant No. JP17H06094) and a Grant-in-Aid for Scientific Research on Innovative Areas (Grant No. JP19H05788) from the Japan Society for the Promotion of Science (JSPS), and the "Nanotechnology Platform" from MEXT, Japan. The authors gratefully acknowledge the Electron Microscopy Laboratory at Peking University for the use of electron microscopes.

*Corresponding author.
p-gao@pku.edu.cn

[1] J. Schooley, W. Hosler, and M. L. Cohen, Phys. Rev. Lett. **12**, 474 (1964).
[2] A. Ohtomo and H. Y. Hwang, Nature (London) **427**, 423 (2004).
[3] A. Rubano, D. Paparo, M. Radović, A. Sambri, F. M. Granozio, U. Scotti di Uccio, and L. Marrucci, Appl. Phys. Lett. **92**, 021102 (2008).
[4] D. Kan, T. Terashima, R. Kanda, A. Masuno, K. Tanaka, S. Chu *et al.*, Nat. Mater. **4**, 816 (2005).
[5] U. Aschauer and N. A. Spaldin, J. Phys. Condens. Matter **26**, 122203 (2014).
[6] S. K. Mishra, R. Ranjan, D. Pandey, P. Ranson, R. Ouillon, J.-P. Pinan-Lucarre, and P. Pruzan, J. Solid State Chem. **178**, 2846 (2005).
[7] J. Gazquez, M. Stengel, R. Mishra, M. Scigaj, M. Varela, M. A. Roldan, J. Fontcuberta, F. Sanchez, and G. Herranz, Phys. Rev. Lett. **119**, 106102 (2017).
[8] P. A. Fleury, J. F. Scott, and J. M. Worlock, Phys. Rev. Lett. **21**, 16 (1968).
[9] L. F. Mattheiss, Phys. Rev. B **6**, 4740 (1972).
[10] E. Heifets, E. Kotomin, and V. A. Trepakov, J. Phys. Condens. Matter **18**, 4845 (2006).
[11] M. Choi, F. Oba, Y. Kumagai, and I. Tanaka, Adv. Mater. **25**, 86 (2013).
[12] H. Katsu, H. Tanaka, and T. Kawai, Jpn. J. Appl. Phys. **39**, 2657 (2000).
[13] M. Itoh, R. Wang, Y. Inaguma, T. Yamaguchi, Y. J. Shan, and T. Nakamura, Phys. Rev. Lett. **82**, 3540 (1999).
[14] J. Haeni, P. Irvin, W. Chang, R. Uecker, P. Reiche, Y. Li *et al.*, Nature (London) **430**, 758 (2004).
[15] D. Lee, H. Lu, Y. Gu, S.-Y. Choi, S.-D. Li, S. Ryu *et al.*, Science **349**, 1314 (2015).
[16] X. Li, T. Qiu, J. Zhang, E. Baldini, J. Lu, A. M. Rappe, and K. A. Nelson, Science **364**, 1079 (2019).
[17] T. Nova, A. Disa, M. Fechner, and A. Cavalleri, Science **364**, 1075 (2019).
[18] O. Tikhomirov, H. Jiang, and J. Levy, Phys. Rev. Lett. **89**, 147601 (2002).
[19] E. Bousquet, M. Dawber, N. Stucki, C. Lichtensteiger, P. Hermet, S. Gariglio, J. M. Triscone, and P. Ghosez, Nature (London) **452**, 732 (2008).
[20] H. W. Jang, A. Kumar, S. Denev, M. D. Biegalski, P. Maksymovych, C. W. Bark *et al.*, Phys. Rev. Lett. **104**, 197601 (2010).
[21] K. Szot, W. Speier, R. Carius, U. Zastrow, and W. Beyer, Phys. Rev. Lett. **88**, 075508 (2002).
[22] M. Choi, F. Oba, and I. Tanaka, Phys. Rev. Lett. **103**, 185502 (2009).
[23] P. Gao, S. Yang, R. Ishikawa, N. Li, B. Feng, A. Kumamoto, N. Shibata, P. Yu, and Y. Ikuhara, Phys. Rev. Lett. **120**, 267601 (2018).
[24] H. Yang, H. S. Lee, M. C. Sarahan, Y. Sato, M. Chi, P. Moeck, Y. Ikuhara, and N. D. Browning, Philos. Mag. **93**, 1219 (2013).
[25] See Supplemental Material at http://link.aps.org/supplemental/10.1103/PhysRevLett.126.225702 for detailed images, EELS and GPA analyses, etc., which includes Ref. [26].
[26] M. J. Hÿtch, E. Snoeck, and R. Kilaas, Ultramicroscopy **74**, 131 (1998).
[27] I. Lazic, E. G. T. Bosch, and S. Lazar, Ultramicroscopy **160**, 265 (2016).
[28] N. Gauquelin, K. H. W. van den Bos, A. Beche, F. F. Krause, I. Lobato, S. Lazar, A. Rosenauer, S. Van Aert, and J. Verbeeck, Ultramicroscopy **181**, 178 (2017).

[29] X. Li, L. Yin, Z. Lai, M. Wu, Y. Sheng, L. Zhang *et al.*, Natl. Sci. Rev. **7**, 755 (2020).
[30] P. Gao, R. Ishikawa, B. Feng, A. Kumamoto, N. Shibata, and Y. Ikuhara, Ultramicroscopy **184**, 217 (2018).
[31] G. Kothleitner, M. J. Neish, N. R. Lugg, S. D. Findlay, W. Grogger, F. Hofer, and L. J. Allen, Phys. Rev. Lett. **112**, 085501 (2014).
[32] K. Uchida, S. Tsuneyuki, and T. Schimizu, Phys. Rev. B **68**, 174107 (2003).
[33] A. Y. Borisevich, A. R. Lupini, J. He, E. A. Eliseev, A. N. Morozovska, G. S. Svechnikov *et al.*, Phys. Rev. B **86**, 140102(R) (2012).
[34] N. Sai and D. Vanderbilt, Phys. Rev. B **62**, 13942 (2000).
[35] K. Müller, W. Berlinger, and F. Waldner, Phys. Rev. Lett. **21**, 814 (1968).
[36] G. Shirane and Y. Yamada, Phys. Rev. **177**, 858 (1969).
[37] L. Fitting, S. Thiel, A. Schmehl, J. Mannhart, and D. A. Muller, Ultramicroscopy **106**, 1053 (2006).
[38] J. P. Buban, M. Chi, D. J. Masiel, J. P. Bradley, B. Jiang, H. Stahlberg, and N. D. Browning, J. Mater. Res. **24**, 2191 (2009).
[39] D. A. Muller, N. Nakagawa, A. Ohtomo, J. L. Grazul, and H. Y. Hwang, Nature (London) **430**, 657 (2004).
[40] R. Brydson, H. Sauer, W. Engel, and F. Hofer, J. Phys. Condens. Matter **4**, 3429 (1992).
[41] A. Ohtomo, D. Muller, J. Grazul, and H. Y. Hwang, Nature (London) **419**, 378 (2002).
[42] E. Stoyanov, F. Langenhorst, and G. Steinle-Neumann, Am. Mineral. **92**, 577 (2007).
[43] M. Li, J. Li, L. Q. Chen, B. L. Gu, and W. Duan, Phys. Rev. B **92**, 115435 (2015).
[44] A. Schiaffino and M. Stengel, Phys. Rev. Lett. **119**, 137601 (2017).
[45] S. Van Aert, S. Turner, R. Delville, D. Schryvers, G. Van Tendeloo, and E. K. Salje, Adv. Mater. **24**, 523 (2012).
[46] M. Kim, G. Duscher, N. D. Browning, K. Sohlberg, S. T. Pantelides, and S. J. Pennycook, Phys. Rev. Lett. **86**, 4056 (2001).
[47] S. Y. Choi, S. D. Kim, M. Choi, H. S. Lee, J. Ryu, N. Shibata *et al.*, Nano Lett. **15**, 4129 (2015).
[48] M. Kim, G. Duscher, N. D. Browning, K. Sohlberg, S. T. Pantelides, and S. J. Pennycook, Phys. Rev. Lett. **86**, 4056 (2001).
[49] D. Marrocchelli, L. Sun, and B. Yildiz, J. Am. Chem. Soc. **137**, 4735 (2015).
[50] J. Luo, J. Materiomics **1**, 22 (2015).
[51] K. D. Johnson and V. P. Dravid, Appl. Phys. Lett. **74**, 621 (1999).